Evaluating constitutive scaling models for application to compressible microflows

Lynne O'Hare [a], Thomas J. Scanlon [a], David R. Emerson [b] and Jason M. Reese [a,*]

[a] *Department of Mechanical Engineering, University of Strathclyde, Glasgow G1 1XJ, UK*

[b] *Centre for Microfluidics and Microsystems Modelling, Daresbury Laboratory, Warrington WA4 4AD, UK*

Abstract

We demonstrate here, for the first time, the constitutive scaling approach applied to simulate a fully compressible, non-isothermal micro gas flow within a mainstream computational physics framework. First, the physics underlying these new constitutive-relation scaling models for rarefied gas flows at the microscale, in particular, the Knudsen layer, is discussed. Results for Couette-type flows in microchannels, including heat transfer effects due to rarefaction, are then reported and we show comparisons with both traditional Navier-Stokes-Fourier solutions and independent numerical studies. We discuss the limitations of the constitutive scaling process, such as the breakdown of the model as the Knudsen number increases and the influence of the wall interaction model on the numerical results. Advantages of the constitutive scaling technique are described, with particular reference to the practicality of using it for microscale engineering design.

Key words: Gas MEMS, Knudsen layer, compressible flow, heat transfer.

* Corresponding author. Tel: +44 141 548 3131.
Email address: jason.reese@strath.ac.uk (Jason M. Reese).

1 Introduction

At the macroscale, engineers routinely use computational fluid dynamics (CFD) methods to design fluid flow and heat transfer systems. However, at the microscale, where rarefaction becomes significant, gas flows are often highly non-equilibrium in nature and are no longer adequately represented by the Navier-Stokes-Fourier (N-S-F) equations of continuum fluid dynamics. New and innovative numerical models must therefore be developed in order to capture the complex rarefaction behaviour observed at very small physical scales.

In this paper we demonstrate, for the first time, the use of constitutive scaling for fully-compressible, non-isothermal flows in CFD. Constitutive scaling is a phenomenological method, in which the constitutive relations traditionally used with the N-S-F equations are replaced by modified functions, curve-fitted from fundamental kinetic theory and direct simulation Monte-Carlo (DSMC) results. Scaling the constitutive relations allows us to represent the gross non-linear behaviour of gas flows near solid interfaces, known as Knudsen layers, where intermolecular collisions do not equilibrate energy and momentum between a gas and its bounding surfaces.

We implement constitutive scaling for both the momentum and energy equations within a conventional CFD application, with a range of boundary conditions appropriate to rarefied flows. Then we discuss the practical implications of using this type of analysis for Couette-type flows in micro-channel geometries, and investigate a range of shear-driven gas flows between parallel plates with coupled heat transfer effects. Our results are shown, and validated against kinetic theory and DSMC as appropriate, and we discuss the relative merits of the constitutive scaling functions we have implemented. Aspects of the simulation are discussed, such as its numerical implementation, wall-normal shear stress variation, predicted Knudsen layer structure, and other features of the analysis specific to modelling the combined transfer of energy and momentum in small-scale gas flows. We then draw conclusions as to the practicality of using the constitutive scaling approach for engineering design, and we outline avenues of future research to extend the applicability of the technique.

2 Physics of Rarefied Flows

At the macroscale the N-S-F equations can predict gas flow and heat transfer properties in a wide variety of situations. These continuum-type equations are only suitable, however, for small departures from the equilibrium state. In microscale applications, large departures from local thermodynamic equilibrium are common, as gas flows in small-scale systems may be rarefied even at atmospheric operating pressures. Rarefaction in small-scale systems is attributable to the magnitude of the molecular mean free path of the gas flow relative to the physical system scale. Typically, rarefaction is characterised by the Knudsen number, which is the dimensionless ratio of the molecular mean free path of the gas, λ, to a characteristic system dimension, H:

$$Kn = \frac{\lambda}{H}, \tag{1}$$

where the equilibrium molecular mean free path of the gas is defined here for hard-sphere molecules as

$$\lambda = \frac{\mu}{\rho}\sqrt{\frac{\pi}{2RT}}. \tag{2}$$

For Kn values less than 0.001, the N-S-F equations remain valid. In the range $0.001 < Kn < 0.1$, boundary conditions that account for discontinuities of momentum and energy between solid surfaces and the gas flow (non-equilibrium flow features known as "slip" and "jump", respectively) may be used with the N-S-F equations. Using this approach, it is possible to model weakly-rarefied flows, although accuracy is limited by the N-S-F equations' inherent inability to predict the nonlinear structure of the Knudsen layer (see below).

Throughout this paper Maxwell's velocity slip boundary condition will be used, including the effects of thermal creep [1]:

$$\overrightarrow{u}_{\text{slip}} - \overrightarrow{u}_{\text{wall}} = \zeta_{\text{slip}}\left(\frac{2-\sigma_U}{\sigma_U}\right)\frac{\lambda}{\mu}\overrightarrow{\tau} + \frac{3}{4}\frac{\Pr\left(\gamma-1\right)}{\gamma P}\overrightarrow{q}, \tag{3}$$

where the tangential shear stress is $\overrightarrow{\tau} = \left(\overrightarrow{i}_n \cdot \Pi\right) \cdot \left(\mathbf{1} - \overrightarrow{i}_n \overrightarrow{i}_n\right)$ and heat flux is $\overrightarrow{q} = \overrightarrow{Q} \cdot \left(\mathbf{1} - \overrightarrow{i}_n \overrightarrow{i}_n\right)$, with an arrow denoting a vector quantity. The slip coefficient ζ_{slip}, equal to 1 in Maxwell's original derivation, is taken to be ≈ 0.8 when constitutive-relation scaling methods are used (as described below) because this value better approximates the true slip magnitude for gas flow over planar surfaces [2]. For temperature jump at solid boundaries,

Smoluchowski's description is used [3]:

$$T_{\text{jump}} - T_{\text{wall}} = \zeta_{\text{jump}} \left(\frac{2 - \sigma_T}{\sigma_T} \right) \left(\frac{2\gamma}{\gamma + 1} \right) \frac{\lambda}{\text{Pr}} \frac{\partial T}{\partial n}. \tag{4}$$

The temperature jump coefficient, ζ_{jump}, is also taken to be ≈ 0.8 when constitutive scaling is used and, again, this value is derived from linearised kinetic theory for gas flow over planar surfaces [4].

Both Maxwell's and Smoluchowski's equations contain phenomenological accommodation coefficients. In the velocity slip case, the tangential momentum accommodation coefficient σ_U determines the proportion of molecules reflected specularly (equal to $1 - \sigma_U$) or diffusely (simply σ_U). The energy accommodation coefficient σ_T has a similar effect, prescribing the degree of energy exchange with the wall. Specular reflection implies that the tangential molecular momentum is unchanged, and that the gas therefore exerts no tangential stress on the wall. It is also assumed that no energy exchange takes place between the wall and the molecule. In the case of diffuse reflection, molecules are ascribed random velocities with the loss of all of their tangential momentum on average, and recede at the temperature of the wall.

At Knudsen numbers greater than 0.1, gas flows are said to be transitional; increasingly fewer intermolecular collisions take place in a given time period, until the flow becomes free-molecular in nature beyond $Kn \approx 10$ [5]. Close to solid surfaces, rarefaction effects are compounded by the relatively large differences in momentum and energy between wall molecules and gas molecules. Although there will be a layer of gas where perfect equilibrium is not attained within one or two mean free paths of a wall in *any* gas based system, it is the increased relative size of the mean free path in rarefied flows that is important. In this near-wall region, known as the Knudsen layer, strong departures from the linear stress/strain-rate (or heat-flux/temperature-gradient) profile predicted by the N-S-F equations are observed.

In very small geometries, where Kn is large, it is possible for the entire flowfield to exhibit nonlinear behaviour, as the Knudsen layers extending from each wall begin to overlap. This can drastically impact macroscopic quantities of engineering interest, such as mass flowrate and drag force. As this occurs, the linear constitutive relationships for shear stress and heat flux used in the N-S-F equations become increasingly unsuitable.

3 Constitutive-Relation Scaling

Relatively-high Knudsen number flows may be simulated using continuum fluid dynamics approaches, provided suitable modifications are made to incorporate at least some of the nonlinear Knudsen layer effects.

One approach is to use a boundary condition that is second-order in Kn. For planar flows, this condition has the form:

$$u_{\text{slip}} = \pm F_1 \lambda \frac{dU}{dn} - F_2 \lambda^2 \frac{d^2U}{dn^2}. \tag{5}$$

This technique has been used with some success by several authors (see, e.g., [6]) to predict certain bulk properties, such as mass flow rates. Its main advantage is that it is simple to implement but, as discussed in [7], there is no consensus on the two coefficients F_1 and F_2, which makes it difficult to create a general model. A more promising approach was proposed in [8], where a second-order set of boundary conditions was derived from the Burnett equations (which are constitutive relations second-order in Kn). However, most of these second-order methods fail to capture the nonlinear features found in Knudsen layers and, moreover, tend to overpredict the slip velocity at the wall.

Instead, the technique we investigate in this paper is the method of constitutive-relation scaling developed by Lockerby *et al.* [2]. This technique uses linearised kinetic theory results to determine a phenomenological function $f(n/\lambda)$ with which to scale the constitutive relationship for shear stress in planar flows, i.e.

$$\tau = \mu \frac{dU}{dn} \Longrightarrow \tau = \frac{1}{f(n/\lambda)}\, \mu \frac{dU}{dn}. \tag{6}$$

The scaling is dependent on normal distance to the nearest solid surface, n, and the local mean free path, λ:

$$f(n/\lambda) \approx 1 + \frac{7}{10}\left(1 + \frac{n}{\lambda}\right)^{-3}. \tag{7}$$

While this specific $f\,(n/\lambda)$ is derived from kinetic theory, it is equally possible to use DSMC, molecular dynamics (MD) or experimental data to determine other case-specific scaling functions, allowing the constitutive scaling method to be extended, in principle, to flows of e.g. polyatomic gases.

This particular constitutive scaling model is derived from a solution for a relatively low speed, planar flow of monatomic gas subject to uniform shear stress.

While its applicability should therefore be limited to cases of this general type, it has been shown to provide reasonably accurate results for some cases that are technically beyond the scope of its derivation [9].

However, the primary advantage of constitutive scaling is that it is an efficient method for incorporating some important rarefaction effects within a continuum framework. It is much less computationally expensive than DSMC or MD, and the method is integrable into conventional engineering tools such as CFD. This means it has significant potential advantages for the practical design of gas-based microsystems.

Several different scaling functions for rarefied micro-flows have been proposed recently: Kn-dependent functions [10], and power-law scaling [11], amongst others [12]. In this paper, however, we discuss the models proposed by Lockerby *et al.* [2] and Reese *et al.* [4]. These will be referred to as Model A and Model B, respectively. The main difference between these two models is the relationship between the constitutive scaling functions for shear stress and for heat flux.

Model A [2]: The function in Eq. (7) is taken alongside the dynamic viscosity to form an *effective* viscosity term that varies with normal distance to the nearest solid surface, i.e.

$$\mu_{\mathrm{eff}_A} = \frac{\mu}{f\left(n/\lambda\right)}, \tag{8}$$

where the subscript A refers to a quantity used in Model A. Then, using the definition of Prandtl number, which describes the relationship between momentum diffusivity and energy diffusivity, i.e.

$$\mathrm{Pr} = \frac{\mu c_p}{\kappa}, \tag{9}$$

an expression for scaling the thermal conductivity, κ, can be found: given the hard-sphere, monatomic gas model condition of $\mathrm{Pr} = 2/3$, then

$$\kappa_{\mathrm{eff}_A} = \frac{\mu_{\mathrm{eff}_A} c_p}{\mathrm{Pr}} = \frac{3}{2}\mu_{\mathrm{eff}_A} c_p. \tag{10}$$

So, in Model A the relative magnitudes of the momentum and energy diffusivities are preserved from the original molecular model. This scaling function has been successfully applied to several standard benchmark micro-flows, includ-

ing Couette flow, Poiseuille flow, flow over an unconfined sphere [2], in addition to cylindrical Couette flow [9] and flow in constricted microchannels [13].

Model B [4]: Constitutive scaling functions for Knudsen layers of both momentum and energy were recently proposed in [4], using kinetic theory data from a wide literature survey to determine effective values of both dynamic viscosity and thermal conductivity. The expressions for these effective quantities are of a similar general form, with the original constitutive constants scaled by normal distance to the nearest wall and the appropriate accommodation coefficient for tangential momentum or energy.

From [14], the replacement constitutive relationship for momentum (i.e. effective viscosity) is:

$$\mu_{\mathrm{eff}_B}(n) = \frac{\mu}{1 - A_{KP}\left(D_{KP}\cdot\sigma_U + E_{KP}\right)\left(1 + \frac{\sqrt{\pi}}{2}\frac{n}{\lambda}\right)^{A_{KP}-1}}, \tag{11}$$

and the scaling function for energy (i.e. effective thermal conductivity) is:

$$\kappa_{\mathrm{eff}_B}(n) = \frac{\kappa}{1 - A_{TJ}\left(D_{TJ}\cdot\sigma_T + E_{TJ}\right)\left(1 + \frac{\sqrt{\pi}}{2}\frac{n}{\lambda}\right)^{A_{TJ}-1}}. \tag{12}$$

The subscripts KP and TJ refer to Kramers' problem and the temperature jump problem, which were the kinetic-theoretical case studies used in the curve-fitting to derive the scaling functions; A, D and E are constants generated in the curve-fitting process, listed in Table 1 for the hard-sphere molecular model. Note that in this model the diffusivities of momentum and energy are *not* both scaled in the same way.

μ-scaling	A_{KP}	D_{KP}	E_{KP}	σ_U
Coeff. value	-2.719	-0.293	0.531	1.0
κ-scaling	A_{TJ}	D_{TJ}	E_{TJ}	σ_T
Coeff. value	-2.142	-0.745	1.295	1.0

Table 1
Coefficients used in Eqs. 11 and 12 to define the scaling functions of Model B.

The scaled diffusive quantities in Model A and Model B are purely *effective* values, and are not intended to be used to define physical values of, for example,

mean free path or Prandtl number. Rather, the original viscosity and thermal conductivity should be used to define physical quantities. Within a CFD framework, however, it is important that physical quantities are retrievable from the scaled model. For example, in the hard-sphere model approximation of monatomic gases, flows incorporating both momentum and energy fluxes may be shown to have a constant Prandtl number, $\mathrm{Pr} = 2/3$ [15]. If this value is not recovered using the "true" velocity or temperature profiles produced by the scaling approach, it is possible that this is due to a physical inconsistency in the scaling model.

Comparing Models A and B: Figures 1 and 2 illustrate the variation of effective dynamic viscosity μ_{eff} and effective thermal conductivity κ_{eff}, compared to nominal constant values of μ and κ, respectively. Model A scales consistently for both dynamic viscosity and thermal conductivity, producing effective quantities 0.59 times their original value at the wall, and reaching the full value of the original quantity outside the Knudsen layer region. Model B is seen to apply different scaling to each quantity, resulting in wall values of $\mu_{\mathrm{eff}} = 0.62\mu$ and $\kappa_{\mathrm{eff}} = 0.47\kappa$, and again reaching the full original value outwith the near-wall region of the flow.

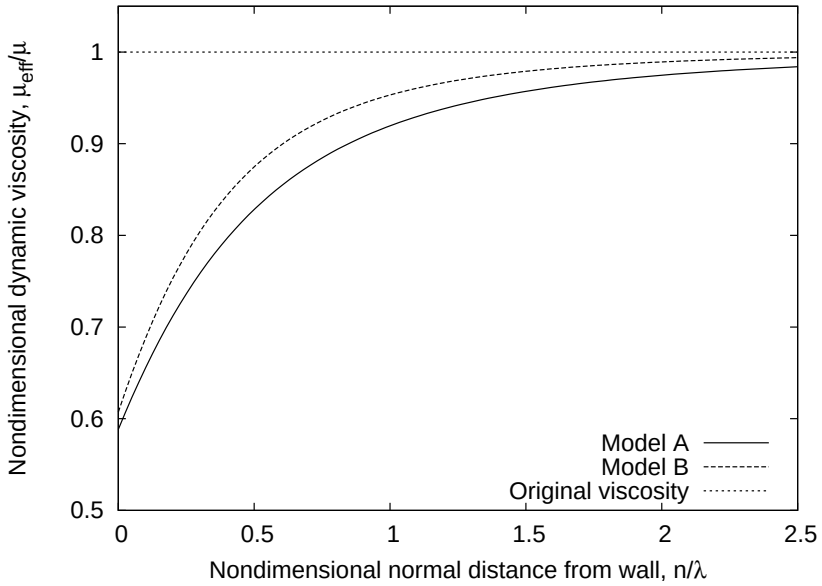

Fig. 1. Effective viscosities provided by the scaling models, compared to (constant) nominal viscosity.

Figure 3 shows the ratio of effective viscosity to effective thermal conductivity predicted by each scaling model, which is directly comparable to the effective

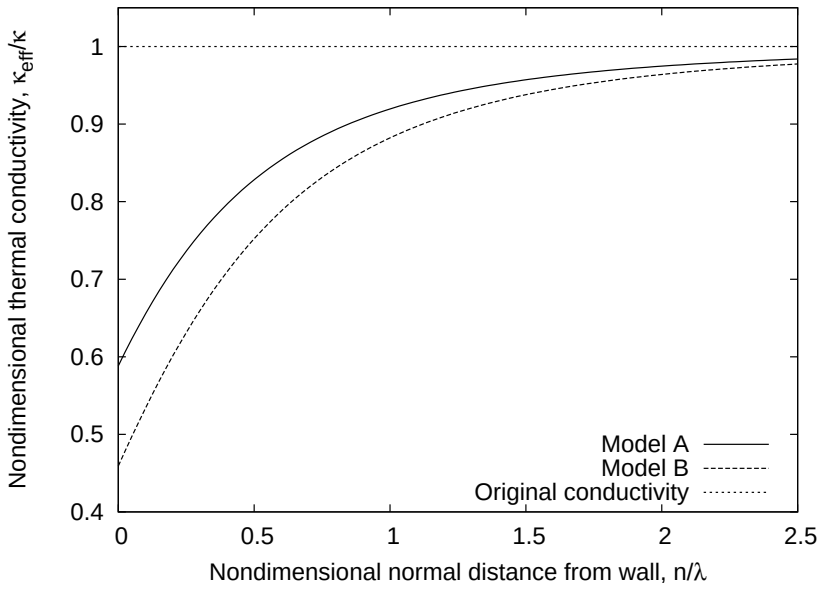

Fig. 2. Effective thermal conductivities provided by the scaling models, compared to (constant) nominal thermal conductivity.

Prandtl number (i.e. Pr from Eq. 9, but using effective quantities and without the specific heat at constant pressure c_p as a coefficient). In the hard-sphere molecular model, only translatory exchanges of energy are present, leading to a fixed ratio of momentum to thermal energy exchange for a fixed collision time, which in turn leads to the constant Prandtl number condition. What the figure illustrates is that using Model B effectively induces a difference between the magnitude of momentum exchange and energy exchange in any given collision. This violates the constant Prandtl number condition of the hard-sphere gas model — which was the model from which the function in Eq. (12) was derived. As such, we conclude that the use of Model B may be inappropriate in cases where both momentum and energy exchange are considered. In isothermal or isoflux cases, however, Model B could still represent a legitimate form of constitutive scaling.

4 Half-Space Problems

In rarefied flows, velocity slip and temperature jump arise within the Knudsen layer as the difference in the average molecular properties of the wall and those of the gas at the wall. The Knudsen layer thickness is the average distance over which these discontinuities would be equilibrated in a quiescent gas (or in an unheated gas for the thermal case). The Knudsen layer regions are illustrated

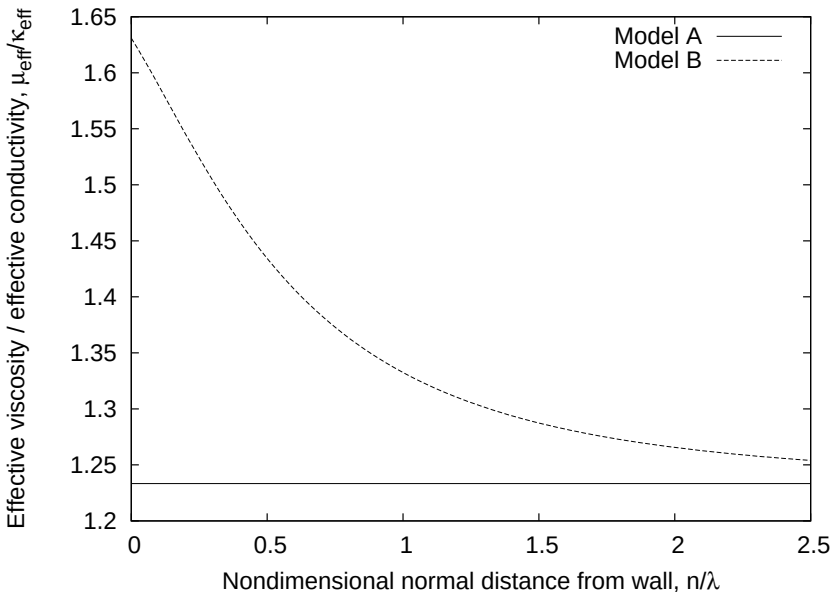

Fig. 3. Ratio of effective viscosity to effective thermal conductivity (ratio of momentum to energy diffusivity) provided by the scaling models.

schematically in Figs. 4 and 5 as extending $\approx 2\lambda$ from the planar surface.

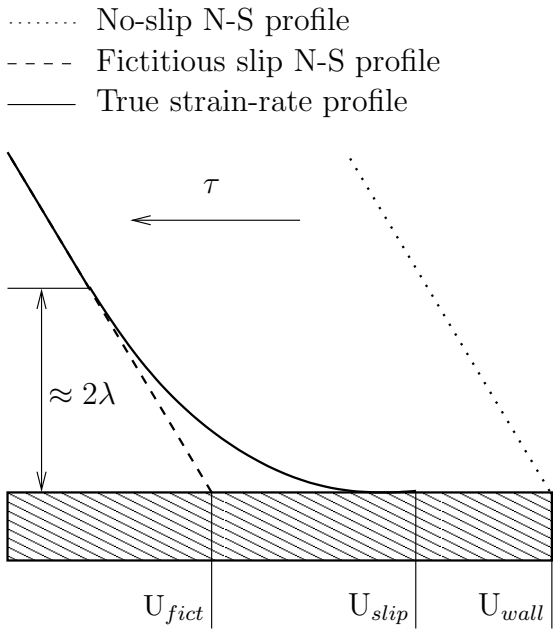

Fig. 4. Schematic of Kramers' problem flow configuration showing constant applied shear stress, τ; traditional, no-slip N-S solution (dotted line), N-S solution with fictitious slip boundary condition (dashed line) and true velocity profile (solid line).

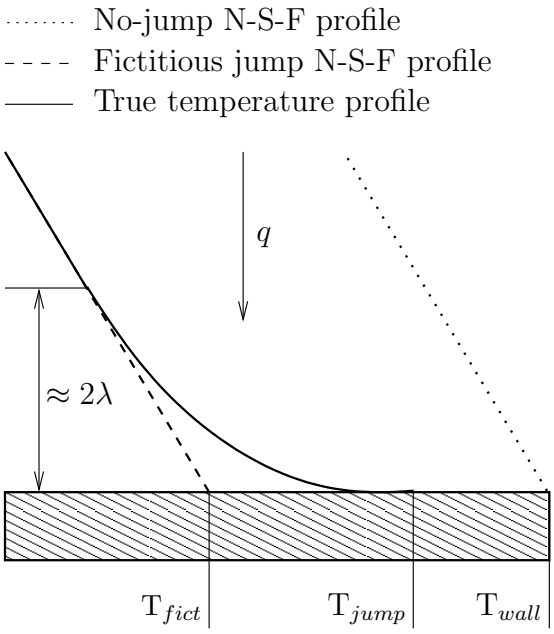

Fig. 5. Schematic of the temperature jump problem showing constant applied heat flux, q; traditional, no-jump N-S-F solution (dotted line), N-S-F solution with fictitious jump boundary condition (dashed line) and true temperature profile (solid line).

4.1 Kramers' problem

Kramers' problem (Fig. 4) is the incompressible, isothermal flow of a gas in a half-space under a constant shear stress that is applied tangentially to a stationary planar wall. The shear stress generates a linear strain-rate profile normal to the wall, except in the near-wall Knudsen layer region where an increase in strain-rate is observed. This momentum Knudsen layer arises due to incomplete accommodation of momentum with the surface.

Although relatively few experimental results are available for constant-shear problems, there are many reliable kinetic theory solutions in the published literature. Typically, these solutions report a velocity *defect*, rather than a velocity profile, varying with normal distance to the stationary wall. Velocity defect is taken to be the difference between a standard Navier-Stokes solution to the problem, with a "fictitious" slip coefficient applied, typically $\zeta_{\text{slip}} = 1.146$, and the true velocity profile in the Knudsen layer [16].

In the derivation of Model B, the concept of velocity defect was used to define a dimensionless function $S(n/\lambda)$ describing the spatial structure of the Knudsen layer [14]. This is effectively a *shape defect* term, describing Knudsen layer

changes in the near-wall profiles of given macroscopic quantities of interest, such as velocity or temperature. The profile defects are curve-fit from a wide range of data to establish the coefficients given in Table 1. By re-casting Eq. (7) in the form of Eqs. (11) and (12), it is possible to express Model A in the form of Model B, using coefficient values of $A = -2$, $D = 0$ (i.e. the Model A function is *not* accommodation-coefficient dependent) and $E = 0.35$. Combining Eqs. (9) and (11) in ref. [4], we then establish

$$S(n/\lambda) = (D\sigma + E)\left(1 + \frac{\sqrt{\pi}}{2}\frac{n}{\lambda}\right)^A, \tag{13}$$

where σ is the surface accommodation coefficient of either tangential momentum or energy, and the $\sqrt{\pi}/2$ term is introduced to convert between those authors' definition of mean free path and our present definition, Eq. (2). Using the dimensionless shape defect, $S(n/\lambda)$, we are able to compare both constitutive scaling models directly to the kinetic theory data presented in [16], as shown in Fig. 6.

It is obvious from Fig. 6 that the Knudsen layer predicted by Model B is much closer to the kinetic theory data than the structure predicted by Model A. This would imply that, at least in this particular case, Model B would be expected to give more accurate results when applied as a scaling relationship to the Navier-Stokes equations. It is noteworthy, however, that very close to the wall even the curve-fit of Model B fails to capture accurately the gradient of the shape defect, which determines, in practice, the shape of the Knudsen layer.

4.2 The temperature jump problem

The temperature jump problem (Fig. 5) is a constant heat flux in a half-space, applied normally to a planar wall in a quiescent gas. In the thermal Knudsen layer near the solid surface the temperature gradient increases, reflecting the incomplete exchange of thermal energy between the gas and the wall.

The thermal Knudsen layer structures predicted by the constitutive scaling models for the temperature jump problem are shown in Fig. 7, in comparison to kinetic theory data from [17] [1] . Again, the shape defect predicted by Model

[1] Very few data points are given in Loyalka's paper. However, the authors are satisfied that it remains one of the most reliable available sources of data for the

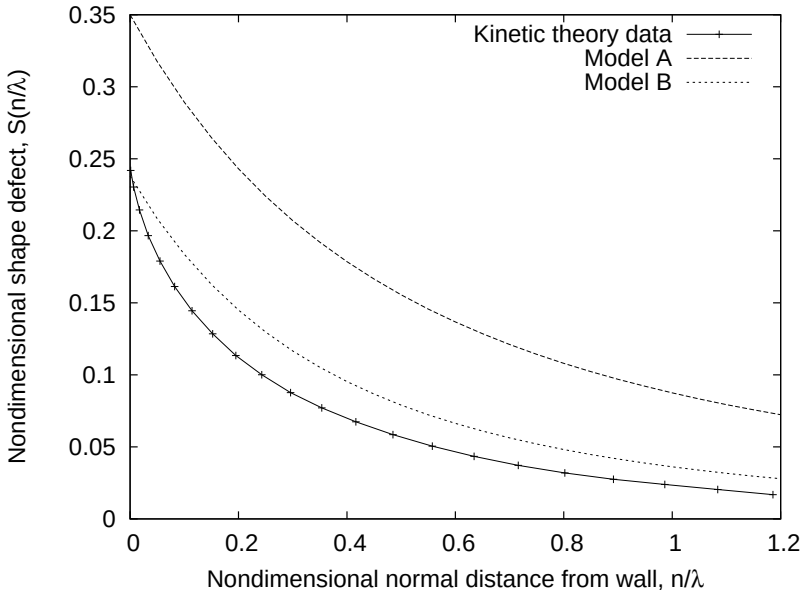

Fig. 6. Knudsen layer shape defect predicted for Kramers' problem: kinetic theory data [16] (points connected by solid line) compared to Model A (dashed line) and Model B (dotted line).

B would seem to provide a much better representation of the thermal Knudsen layer, as observed through the temperature profile. Model A provides a realistic estimate of the shape defect gradient, i.e. the form of the thermal Knudsen layer, but under-predicts the extent of the Knudsen layer (the magnitude of the shape defect).

Considered together, Figs. 6 and 7 illustrate that kinetic models, which only consider transfer of momentum or energy, not both, appear to predict different Knudsen layer structures [16,17]. This difference is the source of the variation in Prandtl number that occurs in Model B. To maintain the monatomic, hard-sphere constant Prandtl number of 2/3, a single Knudsen layer structure, applicable to both momentum and energy transfer, is required — such as that shown by Model A. The Model A trace in Figs. 6 and 7 is roughly equidistant between the Kramers' problem and temperature jump problem profiles, with a gradient that reasonably represents both kinetic theory solutions. It is perhaps for this reason that Model A appears to produce reasonable results across a range of flow configurations [2,9,13], although its original derivation was from an isothermal Kramers' problem case [18].

temperature jump problem.

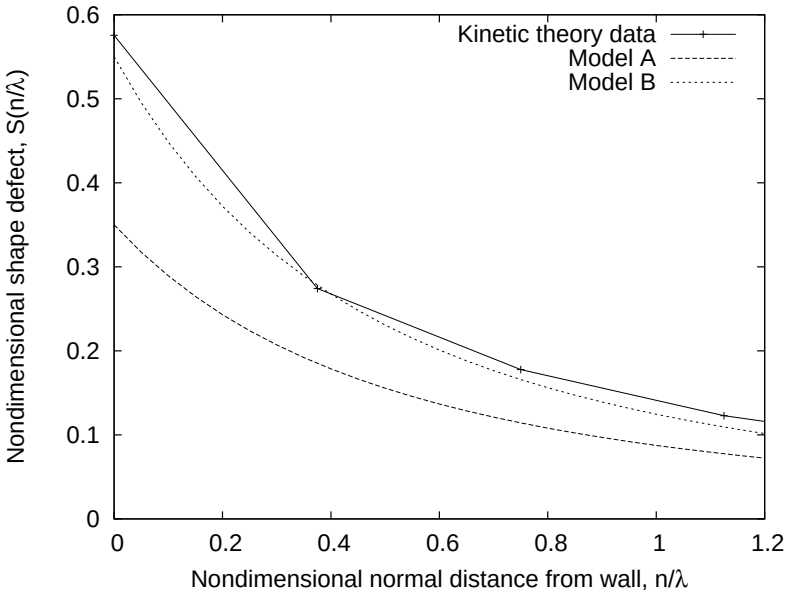

Fig. 7. Knudsen layer shape defect predicted for the temperature jump problem: kinetic theory data [17] (points connected by solid line) compared to Model A (dashed line) and Model B (dotted line).

5 Constitutive Scaling in CFD

In order to create a flexible tool suitable for real-world engineering of gas-based microsystems, we have implemented the constitutive scaling method in the open-source CFD package, OpenFOAM [19]. OpenFOAM is a finite-volume numerics package designed to solve systems of differential equations in arbitrary 3D geometries, using a series of discrete C++ modules. These modules interact to create a series of solvers, utilities and libraries that allow continuum mechanics problems to be pre-processed, solved, and the results post-processed. The advantages of using OpenFOAM as a CFD framework in which to implement constitutive scaling — something that has not been done before for compressible flows — are that the software is both flexible and highly extensible. Its hierarchical, open structure allows the user to make transparent modifications to the governing equations they wish to solve, to tailor them to specific applications whilst retaining the benefits of a stable and general numerical framework.

The particular compressible-flow solver we use in OpenFOAM, developed originally for macroscale rarefied flows, is formulated in terms of density, momentum and total energy. The governing equations are solved in a segregated manner, followed by a PISO-style pressure correction loop. A range of nu-

merical discretisation schemes is employed, with a linear interpolation scheme used throughout to determine face-centre values from cell-centre values.

The scaling of constitutive relationships can be achieved in a CFD code through introducing an effective viscosity and thermal conductivity. We find it convenient to first re-cast the expression for effective viscosity into an expression for effective mean free path based on normal distance to the nearest wall, i.e.

$$\lambda_{\text{eff}} = \frac{\lambda_{\text{original}}}{f\left(n/\lambda_{\text{original}}\right)}. \tag{14}$$

The definition of molecular mean free path, Eq. (2), is then used to define an effective dynamic viscosity:

$$\mu_{\text{eff}} = \frac{\lambda_{\text{eff}}\rho}{\sqrt{\frac{\pi}{2RT}}}. \tag{15}$$

One motivation to do this is that we postulate that in real systems, some changes to the mean free path of the gas would occur in the Knudsen layer region, due both to solid-gas collisions and to the interaction between gas molecules incident to the surface and those reflected from it [20].

However, the primary motivation for the use of an effective mean free path in constitutive scaling models is that the strain-rate in Maxwell's slip Eq. (3), $\overrightarrow{\tau}/\mu$, increases with effective viscosity. However, by including the effective viscosity as a function of mean free path, which is, in turn, a function of wall-normal distance, the true strain-rate at the wall can be used to determine the slip velocity. In constant-shear-stress problems, such as Couette flow, we thereby maintain the correct shear-stress despite the variation in strain-rate observed through the Knudsen layer. This cannot be said of other constitutive scaling implementations, which rely on separate calculation of the viscous stress arising from an equivalent equilibrium strain-rate profile.

6 Compressible Micro-Couette Flow

To demonstrate the use of constitutive scaling in a typical engineering application, we simulate high-speed Couette flow of argon gas in a 2D channel. This is the first application of a constitutive scaling method to fully compressible microflows in CFD. While the system set-up, described below, is isothermal, rarefaction effects generate a temperature profile in the flow; so the flow itself is non-isothermal [21].

The problem we have chosen here is essentially a 1D flow, but we solve it as a 2D planar flow, and our models and solvers have been implemented fully in 3D in OpenFOAM, to enable other more general problems to be investigated in the future.

The 2D channel configuration is shown in Fig. 8. The upper wall remains stationary and the lower wall moves in the positive x-direction at Mach 1 (with the local speed of sound calculated using the wall temperature), generating a constant tangential shear stress. The channel length is a minimum of $60\mu m$, and in any case sufficiently long as to allow end effects to become negligible in the developed flow in the centre of the system. Its height in the y-direction is varied in order to determine the Knudsen number of the case. The different channel heights used are given in Table 2, with corresponding Kn values. For validation purposes, we compare our CFD results up to $Kn = 0.5$ — a relatively large value for constitutive scaling [4] — to DSMC data available in [22].

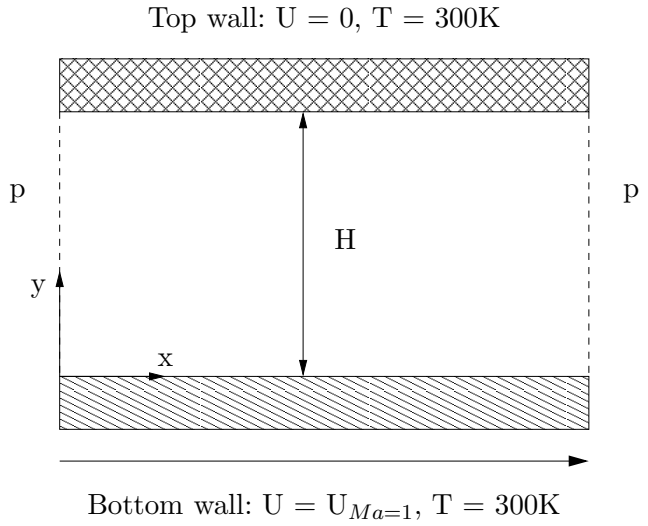

Fig. 8. Couette flow configuration and nomenclature for our compressible CFD analysis; $U_{Ma=1}$ is the velocity applied to move the lower wall at the local speed of sound.

Kn	0.01	0.1	0.2	0.5	0.8
H ($\times 10^{-6}$m)	7.09	0.709	0.3545	0.1418	0.0886

Table 2
Table of channel heights used to vary Kn in our simulations.

Argon gas at a temperature of 300K is used as the working fluid, with both wall temperatures fixed at 300K. The use of argon makes ref. [22] a particularly

appropriate source of validation data: it is a monatomic gas, which is in keeping with the assumptions of molecular behaviour inherent in the velocity slip and temperature jump conditions [23], and in the derivation of the constitutive scaling relationships from hard-sphere molecular force interaction models [2,4].

At the channel ends, a fixed-value boundary condition on pressure is used, $p = 101.325$kPa, and the temperature and velocity gradients normal to the (parallel) inlet and outlet faces are set to zero. Velocity slip and temperature jump boundary conditions (Eqs. 3 and 4) are used at the channel walls; tangential accommodation coefficients of momentum and energy are fixed at $\sigma_U = \sigma_T = 1$, with the slip/jump coefficients $\zeta_{\text{slip}} = \zeta_{\text{jump}} = 0.8$. Structured hexahedral meshes, tested to ensure grid-independent results, are used in all cases. The cell density increases towards the channel walls, in order to capture the Knudsen layer structure accurately.

In combining the transport of both energy and momentum, this shear-driven case exposes weaknesses in Model B:

- The relative diffusivities of energy and momentum for the monatomic hard-sphere model must be fixed by the condition $\text{Pr} = 2/3$ — Model B violates this condition and is therefore, strictly, inappropriate for application to this case;
- For this case, the velocity profiles produced by Model B are near-identical to those of Model A, as illustrated in Fig. 9, while temperature results from Model B are somewhat less accurate than those from Model A (in comparison to DSMC), as illustrated in Fig. 10. While it is important to note that both models capture the same type of temperature profile as predicted by DSMC, with a similar magnitude of the peak (channel-centre) temperature, there are differences between the model results and the DSMC data. These may be attributed to: a) the fact that both models are derived from linear problems, so may not be applicable to Couette flow where the temperature profile is parabolic, and b) that DSMC is able to capture other rarefaction effects, such as tangential heat fluxes, which the present models cannot. (The latter fact may be expected to result in more pronounced divergences between these models and DSMC in simulations of more complicated flow systems.)

Considering these factors, and the limited applicability of Model B in terms of recovering a constant Prandtl number physically, the results we report below are taken from Model A simulations only.

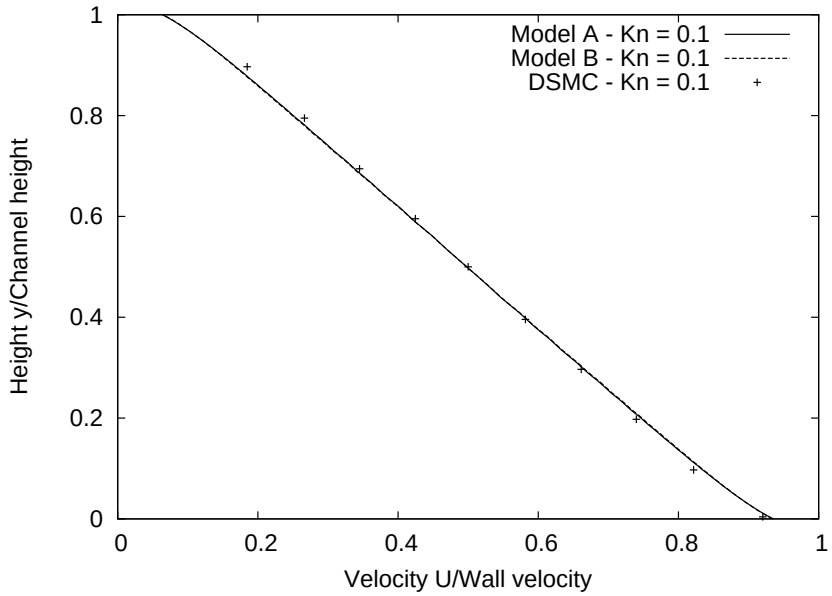

Fig. 9. Micro-Couette velocity profiles predicted by Model A, Model B and DSMC [22] for $Kn = 0.1$.

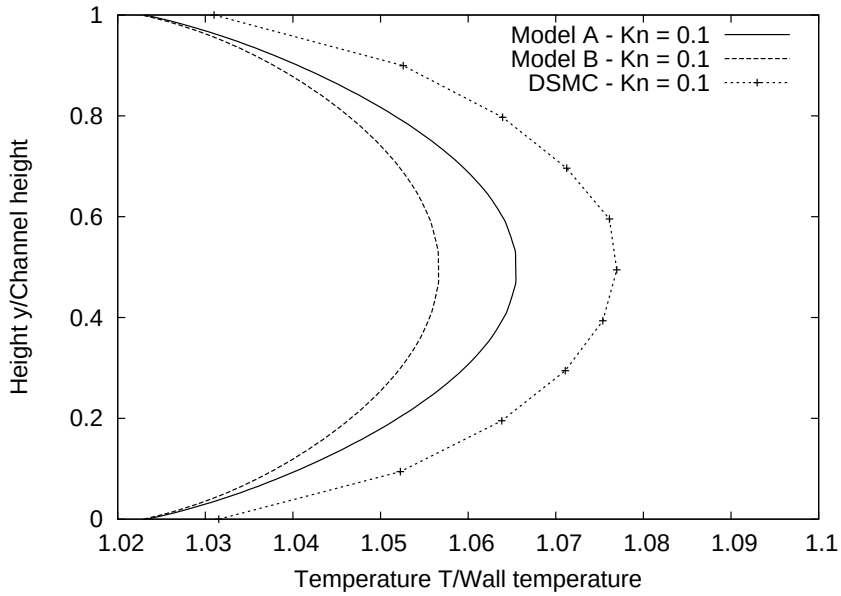

Fig. 10. Micro-Couette temperature profiles predicted by Model A, Model B and DSMC [22] for $Kn = 0.1$.

Figure 11 shows the velocity cross-channel profiles predicted using the CFD implementation of Model A for a range of Kn values (shown as lines), compared to the corresponding DSMC data (shown as points) from [22]. Velocity is non-dimensionalised by the velocity of the moving lower wall; the spatial position in the y-direction is non-dimensionalised by the appropriate channel

height. As the figure illustrates, the Knudsen layer structure is represented relatively well by the CFD, although as Kn increases the deviation from the DSMC data does become more appreciable.

Figure 12 shows temperature profiles in the lower half of the channel for the compressible Couette flow case. Results obtained using Model A are compared to results from the standard form of the N-S-F equations. First, the no-slip, no-jump boundary conditions common to macroscale CFD are used; then, these are replaced with slip and jump boundary conditions from Eqs. (3) and (4). Temperature is non-dimensionalised by the fixed wall temperature. Results are shown for two key Kn values, 0.01 and 0.1, which are close to the lower and upper limits, respectively, of the slip-flow regime [5]. The no-slip/no-jump model is shown as a single solid line, which is the same for both of these Kn values, given that the N-S-F equations fail to predict altered flow profiles with increasing Kn.

The introduction of slip and jump boundary conditions improves the performance of the N-S-F model, but nonlinear Knudsen layer effects remain beyond its scope. As shown in Fig. 12, at the lower limit of the slip regime, the difference between the N-S-F with slip/jump boundary conditions and the constitutive-scaling model is small, and only practically observed as a very slightly increased temperature gradient close to the wall. At this Kn, the scaled equations and the N-S-F equations return near-identical temperature jump values at the wall. As Kn increases to 0.1, the difference between the standard N-S-F model and Model A becomes marked, with Model A predicting lower temperatures across much of the flow, and a noticeably smaller temperature jump at the wall. The temperature gradient is also seen to increase near the wall, reflecting the presence of a thermal Knudsen layer — an effect not captured by the unscaled N-S-F equations, regardless of the boundary conditions applied. This illustrates that even for flows with Kn values traditionally considered to be part of the slip regime, the structure of the Knudsen layer can significantly impact macroscopic quantities of interest. When Kn approaches the upper limit of the slip regime and tends towards the lower limit of the transition regime, it is important that numerical models should capture Knudsen layer behaviour.

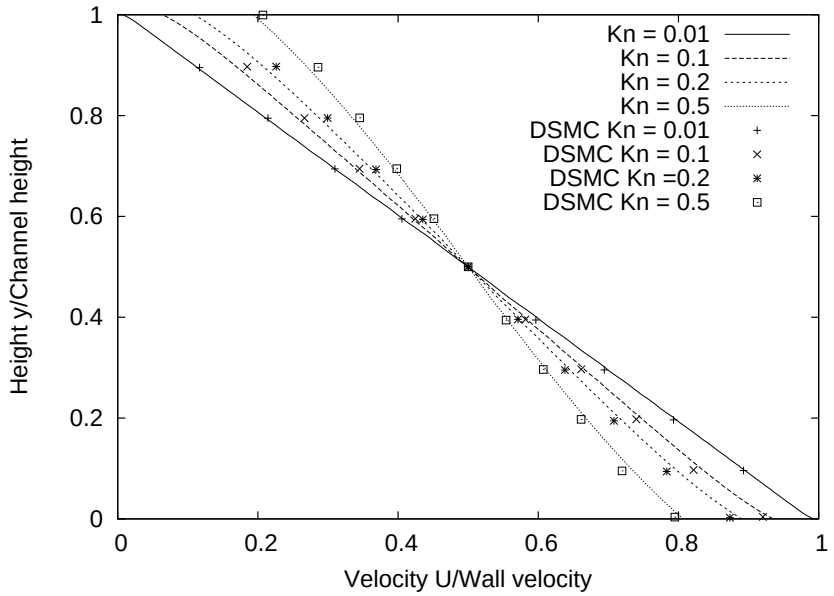

Fig. 11. Compressible micro-Couette flow velocity profiles; comparison of Model A results (lines) to DSMC data (points) [22].

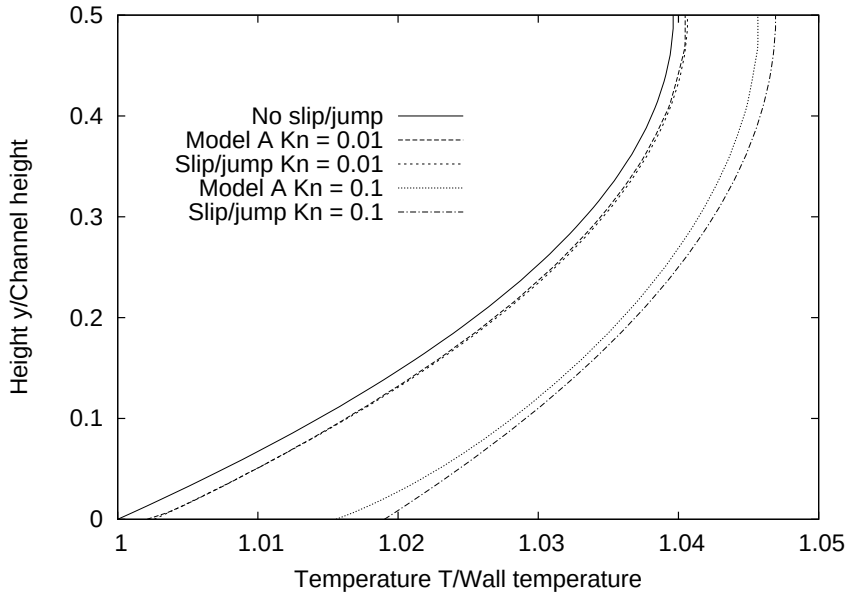

Fig. 12. Compressible micro-Couette flow temperature profiles predicted by Model A.

7 Discussion

One of the primary advantages of constitutive-relation scaling is that it is quite simple to implement but is able to capture some of the trends associated with the complex non-equilibrium physics of the Knudsen layer. When applied to

lower Kn transitional flows, constitutive scaling can offer greatly improved accuracy over simple N-S-F solutions in the prediction of macroscopic quantities of interest, such as mass flowrate [24].

In this paper we have successfully implemented a constitutive scaling approach in conventional CFD. This brings a great deal of flexibility to the method, moving it away from its original "single-user, single-case" scientific basis, towards suitability for use as a design tool for real engineering problems. The successful analysis we have demonstrated of a fully-compressible, non-isothermal case, represents a significant step forward in this respect.

The method could be advanced with the derivation of new scaling models, in place of the models A and B we have investigated. Both of these models are phenomenological in nature, as they are curve-fit from pre-existing (and case-specific) Knudsen layer solutions using other independent methods. They are also derived from kinetic solutions that use only the hard-sphere molecular model. A physical analysis of near-wall intermolecular interactions, and deriving scaling functions from more complex force-interaction laws (e.g. soft-spheres), would provide a more general model.

Certain physical flow features, such as wall-normal shear stresses or tangential heat fluxes, and the Knudsen minimum, seem to be beyond the scope of existing constitutive scaling within an N-S-F framework. While replacing the scaled N-S-F equations with a higher-order continuum model is desirable, no single higher-order equation set has, as yet, demonstrated universal superiority [24]. Higher-order models also require additional boundary conditions, which can be difficult to obtain or prescribe.

While isothermal flow over spheres, Couette flow between rotating cylinders and flow through channels with venturi-type constrictions have all been successfully analysed previously using Model A [2,9,13], it is important to explore the applicability of the model. For example, Fig. 13 shows the temperature profile predicted by Model A for the micro-Couette flow case, with results for the high Kn value of 0.8 included. The CFD initially shows higher maximum temperatures and a more linear profile as Kn increases, comparable to the data available in [22,25]. But lower maximum temperatures start to appear as $Kn \rightarrow 0.5$, or even somewhat lower, as the Knudsen layers from opposite sides of the channel begin to interact with each other, and boundary slip/jump effects increase. Our scaling method effectively prescribes a velocity/temperature gradient dependent only on normal distance from a surface,

and may not properly account for this physical coupling between Knudsen layers. It also makes use of Maxwell's and Smoluchowski's phenomenologically-derived boundary conditions for gas-solid interactions and, as Kn increases, slip/jump effects become dominant, magnifying errors arising at the system boundaries [18].

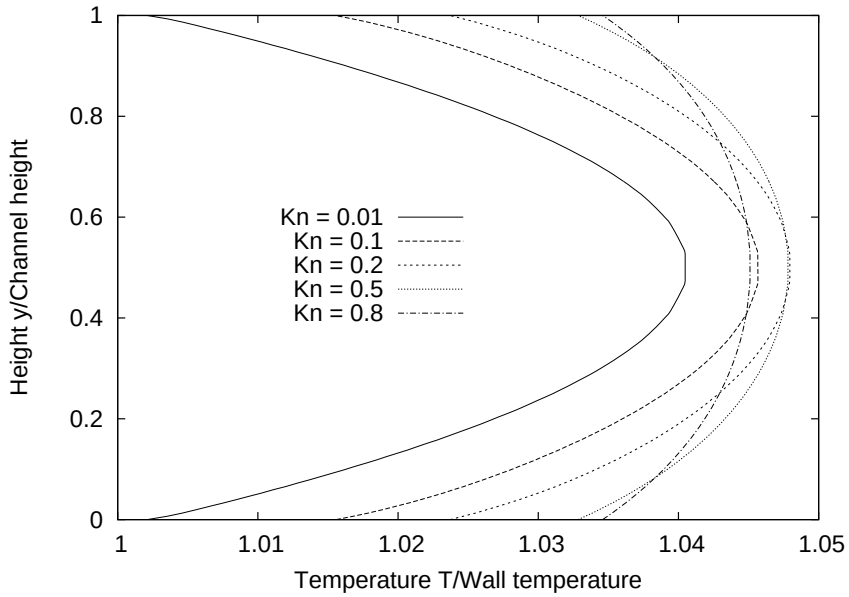

Fig. 13. Temperature profiles predicted by Model A, with high-Kn results.

The temperature profiles produced are, of course, accommodation-coefficient dependent. In order to isolate the slip/jump effects, the compressible micro-Couette flow case detailed above was reassessed using both Model A and the unscaled N-S-F equations, with different combinations of tangential accommodation coefficients for energy and momentum. Two different values of accommodation coefficient were used, first $\sigma = 1$ for comparison to Xue's DSMC [22], then $\sigma = 0.8$, a value typical of argon flows in silicon channels [26]. For both simulation types, four combinations of σ_U and σ_T were used: $\sigma_U = \sigma_T = 1$; $\sigma_U = 0.8$ and $\sigma_T = 1$; $\sigma_U = 1$ and $\sigma_T = 0.8$; and finally $\sigma_U = \sigma_T = 0.8$. In the Model A cases, the true microslip coefficients of $\zeta_{\text{slip}} = \zeta_{\text{jump}} = 0.8$ were used, and in the N-S-F analyses, the standard values of $\zeta_{\text{slip}} = \zeta_{\text{jump}} = 1$ were applied.

Figure 14 shows results from Model A at Kn values of 0.2, 0.5 and 0.8 when $\sigma_U = \sigma_T = 0.8$, comparable to the high-Kn results shown in Fig. 13 where $\sigma_U = \sigma_T = 1$. The decrease in the accommodation coefficients is seen to increase the temperature jump at the wall, and the crossover of the maximum temperature predictions has occurred at a much lower Kn. Therefore, even for

relatively small changes in the tangential accommodation coefficients, large variations in the results of numerical analyses can be observed. As several recent studies have shown low accommodation coefficients to be practically realisable — e.g. σ_U values as low as 0.52, arguably, for carbon nanotubes [27] — different accommodation coefficients, and the accuracy with which they are determined in experimental cases, are likely to have an important effect on many types of continuum models for rarefied gas flow.

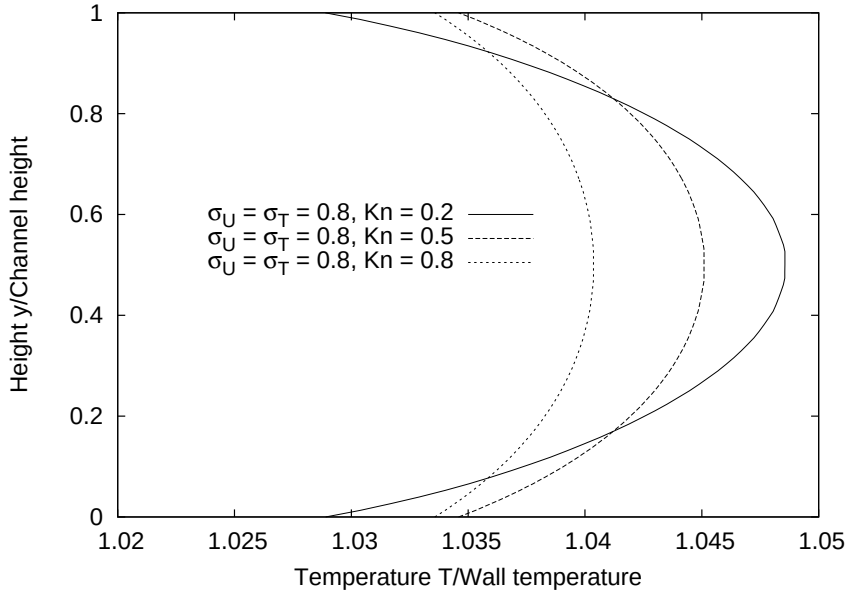

Fig. 14. Temperature profiles predicted by Model A; results as Kn increases while $\sigma_U = \sigma_T = 0.8$.

Also of interest is the interaction between the two types of accommodation coefficient. In N-S-F analyses at high Kn it was found that when energy and momentum accommodation coefficients were equal, at either 0.8 or 1, the predicted temperature jump at the channel walls was relatively similar, as is the predicted maximum temperature at the channel centre. However, if one accommodation coefficient is set to 0.8 and the other to 1, the behaviour of the simulation can be significantly altered.

To illustrate, Fig. 15 shows how the maximum predicted temperature (the temperature at the channel centre) varies with Kn. Each accommodation coefficient combination displays a definite peak in the predicted temperature, occurring in the range of Kn values between about 0.15 and 0.45. The largest maximum temperatures are predicted when the energy accommodation coefficient is at its lowest value of $\sigma_T = 0.8$, with momentum accommodation coefficient $\sigma_U = 1$. Conversely, when the momentum accommodation coeffi-

cient is $\sigma_U = 0.8$, and the energy accommodation remains at $\sigma_T = 1$, the maximum predicted temperature is at its lowest.

As shown in Fig. 15, these highest and lowest maximum temperature profiles are equidistant from the "reference" state where $\sigma_U = \sigma_T = 1$. This implies that energy and momentum are assumed to be exchanged at the same rate when Maxwell's and Smoluchowski's boundary conditions are used simultaneously, which is unlikely to be true of any physical system. For example, returning to our earlier discussion of Prandtl number, we know the momentum diffusivity to be only a proportion of the energy diffusivity, and momentum is exchanged at a faster rate than energy [18]. Accommodation coefficients are not physical properties of a surface, but rather they arise from the interaction between gas and wall molecules, and little is really known about the complex physics of gas flow in near-surface regions. It is therefore likely that more physically-based boundary conditions, such as Langmuir's slip model, based on surface chemistry, would be better suited to many practical micro-engineering flow simulations [28].

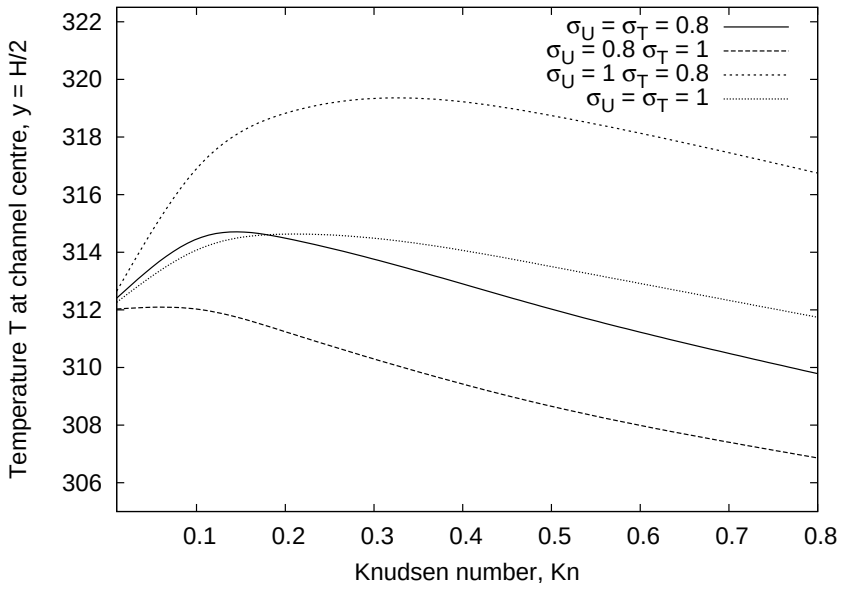

Fig. 15. Predicted temperature (in K) at the centre of the channel in compressible micro-Couette flow (i.e. the maximum temperature), plotted against Knudsen number.

8 Conclusions

In this paper, some of the key physics of rarefied gas flows has been outlined, including the discontinuities of energy and momentum at fluid-solid boundaries, and the behaviour of gas flow in near-wall Knudsen layer regions. The constitutive scaling approach to modelling the Knudsen layer within a conventional continuum fluid dynamics framework has also been described. The relative merits of two available constitutive scaling models have been compared, and the models tested using engineering cases.

We have demonstrated here, for the first time, the integration of a constitutive scaling approach into conventional CFD for fully-compressible, non-isothermal flows, and have compared our technique with independent DSMC results. We have also discussed the practical implications of using this type of simulation approach for microscale gas flows, and have outlined some of its advantages and disadvantages when compared with alternative methods.

Future work will include further investigation of constitutive scaling models, and the development of new, more generally-applicable functions based on analysis of molecular dynamics results for Knudsen layers. We also intend to assess the range of physically-based boundary conditions, and to make use of our current compressible flow CFD implementation as an engineering tool for investigating a number of technological microflow configurations.

Acknowledgements

The authors would like to thank Robert Barber of Daresbury Laboratory, UK, and Yingsong Zheng and Chris Greenshields of the University of Strathclyde, UK, for useful discussions. This research is funded in the UK by the Engineering and Physical Sciences Research Council under grant no. GR/S77196/01.

Nomenclature

A	Scaling coefficient
c_p	Specific heat at constant pressure (kJ/kgK)
D	Scaling coefficient

E	Scaling coefficient
$F_{1,2}$	Coefficients in second-order slip boundary conditions
H	Channel height, characteristic system dimension (m)
Kn	Knudsen number
Ma	Mach number
Pr	Prandtl number
$\mathrm{Pr}_{\mathrm{eff}}(n)$	Effective Prandtl number
$\overrightarrow{Q}$	Heat flux vector at the wall ($\mathrm{W/m^2}$)
R	Specific gas constant (kJ/kg K)
$S(n/\lambda)$	Knudsen layer shape defect
T	Gas temperature (K)
T_{jump}	Temperature jump (K)
T_{wall}	Wall temperature (K)
U	Gas velocity (m/s)
$U_{Ma=1}$	Gas velocity at $Ma = 1$ (m/s)
$f(n/\lambda)$	Scaling function
$\overrightarrow{i}_n$	Unit vector normal to and away from a wall
n	Normal distance away from a wall (m)
p	Pressure (Pa)
$\overrightarrow{q}$	Tangential heat flux ($\mathrm{W/m^2}$)
$\overrightarrow{u}_{\mathrm{slip}}$	Slip velocity (m/s)
$\overrightarrow{u}_{\mathrm{wall}}$	Wall velocity (m/s)
γ	Ratio of specific heats
ζ_{slip}	Velocity slip coefficient
ζ_{jump}	Temperature jump coefficient
κ	Thermal conductivity (W/mK)
κ_{eff_A}	Effective conductivity — Model A (W/mK)
κ_{eff_B}	Effective conductivity — Model B (W/mK)
λ	Equilibrium mean free path of the gas (m)
λ_{eff}	Effective mean free path (m)
$\lambda_{\mathrm{original}}$	Original mean free path (m)
μ	Dynamic viscosity (kg/m s)
μ_{eff_A}	Effective viscosity — Model A (kg/m s)
μ_{eff_B}	Effective viscosity — Model B (kg/m s)
Π	Stress tensor at the wall ($\mathrm{N/m^2}$)
ρ	Gas density ($\mathrm{kg/m^3}$)
σ_U	Tangential momentum accommodation coefficient
σ_T	Tangential energy accommodation coefficient
$\overrightarrow{\tau}$	Tangential shear stress ($\mathrm{N/m^2}$)
$\mathbf{1}$	Identity tensor

References

[1] J.C. Maxwell, *On stresses in rarified gases arising from inequalities of temperature,* Phil. Trans. Roy. Soc., Part 1, **170** (1879) 231–256.

[2] D.A. Lockerby, J.M. Reese and M.A. Gallis, *Capturing the Knudsen layer in continuum-fluid models of non-equilibrium gas flows,* AIAA J., **43** (2005) 1391–1393.

[3] M. von Smoluchowski, *Über wärmeleitung in verdünnten gasen,* Annalen der Physik und Chemie, **64** (1898) 101–130.

[4] J.M. Reese, Y. Zheng and D.A. Lockerby, *Computing the near-wall region in gas micro- and nanofluidics: critical Knudsen layer phenomena,* J. Computational and Theoretical Nanoscience, **4** (2007) 807–813.

[5] M. Gad-el-Hak, *The Fluid Mechanics of Microdevices — The Freeman Scholar Lecture,* J. Fluids Eng. (Trans. ASME), **121** (1999) 5–33.

[6] S. Colin, P. Lalonde and R. Caen, *Validation of a second-order slip flow model in rectangular microchannels,* Heat Transf. Engng., **25** (2004) 23–30.

[7] R.W. Barber and D.R. Emerson, *Challenges in modeling gas-phase flow in microchannels: from slip to transition,* Heat Transf. Engng., **27** (2006) 3–12.

[8] D.A. Lockerby, J.M. Reese, D.R. Emerson and R.W. Barber, *Velocity boundary condition at solid walls in rarefied gas calculations,* Phys. Rev. E, **70** (2004) art. no. 017303.

[9] L. O'Hare, D.A. Lockerby, J.M. Reese and D.R. Emerson, *Near-wall effects in rarefied gas micro-flows: some modern hydrodynamic approaches,* Int. J. Heat and Fluid Flow, **28** (2007) 37–43.

[10] C. Cercignani, A. Frangi, S. Lorenzani and B. Vigna, *BEM approaches and simplified kinetic models for the analysis of damping in deformable MEMS,* Eng. Analysis with Boundary Elements, **31** (2007) 451–457.

[11] C.R. Lilley and J.E. Sader, *Velocity gradient singularity and structure of the velocity profile in the Knudsen layer according to the Boltzmann equation,* Phys. Rev. E, **76** (2007) art. no. 026315.

[12] G.E. Karniadakis, A. Beskok and N. Aluru, *Microflows and Nanoflows: Fundamentals and Simulation,* Springer-Verlag New York Inc. (2005).

[13] L. O'Hare, T.J. Scanlon and J.M. Reese, *Gas flow through microscale orifice plates,* Proceedings of ASME ICNMM2006, **96193** (2007) Limerick, Ireland.

[14] Y. Zheng, J.M. Reese, T.J. Scanlon and D.A. Lockerby, *Scaled Navier-Stokes-Fourier equations for rarefied gas flow and heat transfer phenomena in micro- and nanosystems,* Proceedings of ASME ICNMM2006, **96066** (2007) Limerick, Ireland.

[15] L. Mieussens and H. Struchtrup, *Numerical comparison of Bhatnagar-Gross-Krook models with proper Prandtl number,* Phys. Fluids, **16(8)** (2004) 2797–2813.

[16] C. Cercignani, *Knudsen layers: theory and experiment,* in Recent Developments in Theoretical and Experimental Fluid Dynamics, U. Muller, K.G. Rosner and B. Schmidt eds., Springer-Verlag, Berlin (1979) 187–195.

[17] S.K. Loyalka, *Temperature jump: rigid-sphere gas with arbitrary gas/surface interaction,* Nuclear Sci. Eng., **108** (1991) 69–73.

[18] C. Cercignani, *Mathematical Methods in Kinetic Theory (2^{nd} Edition),* Plenum Press, New York (1990).

[19] OpenFOAM, http://www.openfoam.org.

[20] D.W. Stops, *The mean free path of gas molecules in the transition regime,* J. Phys. D: Appl. Phys., **3** (1970) 685–696.

[21] D.A. Lockerby and J.M. Reese, *High-resolution Burnett simulations of micro Couette flow and heat transfer,* J. Comput. Phys., **188** (2003) 333-347.

[22] H. Xue, H. Ji and C. Shu, *Prediction of flow and heat transfer characteristics in micro-Couette flow*, Microscale Thermophysical Engineering, **7** (2003) 51–68.

[23] E.K. Kennard, *Kinetic Theory of Gases,* McGraw-Hill Book Company Inc. (1938).

[24] D.A. Lockerby, J.M. Reese and M.A. Gallis, *The usefulness of higher-order constitutive relations for describing the Knudsen layer,* Phys. Fluids, **17** (2005) art. no. 100609.

[25] K. Nanbu, *Analysis of the Couette flow by means of the new direct-simulation method*, J. Physical Society of Japan, **52** (1983) 1602–1608.

[26] E.B. Arkilic *Measurement of the mass flow and tangential momentum accommodation coefficient in silicon micromachined channels*, PhD thesis, M.I.T. (1997).

[27] S.M. Cooper, B.A. Cruden, M. Meyyappan, R. Raju and S. Roy, *Gas transport characteristics through a carbon nanotubule*, Nano Letters, **4** No. 2 (2004) 377–381.

[28] R.S. Myong, J.M. Reese, R.W. Barber and D.R. Emerson, *Velocity slip in microscale cylindrical Couette flow: The Langmuir Model*, Phys. Fluids, **17** (2005) art. no. 087105.